# Unsteady-state Computational Fluid Dynamics Modeling of Hydrogen Separation from $H_2/N_2$ Mixture

**Abdolmajid Sharafpoor[1], Zahra Mansourpour[1]* and Azadeh Ghaee[2]**

*1. School of Chemical Engineering, College of Engineering, University of Tehran, Tehran, Iran.*
*2. Department of Life Science Engineering, Faculty of New Science and Technologies, University of Tehran, Tehran, Iran.*

**(Received 2017.05.14, Accepted 2017.11.03)**

## Abstract

3D modeling of Pd/α-Al2O3 hollow fiber membrane by using computational fluid dynamic for hydrogen separation from H2/N2 mixture was considered in steady and unsteady states by using the concept of characteristic time. Characteristic time concept could help us to design and calculate surface to volume ratio and membrane thickness, and adjust the feed conditions. The contribution of resistance between the membrane and the gas phase could be analyzed by considering characteristic times. The effect of temperature on quasi-steady time (t99) was examined at constant feed flow rate and pressure. As a result, when thickness of membrane was less than the critical amount, the surface resistance was important. According to the results, about 50% mass separation was obtained in the initial 8% period of permeation time. By enhancing temperature, membrane permeation and, consequently, hydrogen separation increased. The CFD results showed good agreement with experimental data.

## Keywords

Hollow fiber membrane;
Computational fluid dynamics;
Hydrogen separation;
Characteristic time;
Unsteady state.



## 1. Introduction

The production of ultra-pure hydrogen is required and fuel value of hydrogen is 3.4 times more valuable than chemical feedstock value. For this reason, hydrogen separation has economic justification [1]. The hydrogen-rich gases can be separated by pressure swing adsorption (PSI), cryogenic distillation (CD), and membrane separation [2-3]. Among the mentioned methods, membrane separation has attracted greater attention due to low energy consumption and being suitable for small-to-moderate scale production of hydrogen in comparison with other methods [4]. Researchers are interested in studying the palladium membrane, because separation of ultra-pure hydrogen from gas mixture can be attained by Pd and Pd alloys membrane [5]. The mechanism of hydrogen transfer in palladium membrane is solution diffusion. Pure palladium

* Corresponding Author.
Tel./Fax: +982161112196
Email: mansourp@ut.ac.ir (Z. Mansourpour)

membrane has disadvantages such as: high cost, hydrogen embrittlement, and poor resistance to poisoning by gaseous contamination, such as $H_2S$, CO, and $H_2O$ [6]. For this purpose, to reduce the cost and better utilize the attributes of pure palladium membranes, coated palladium with various supports has been developed [7-9].

Among a variety of membrane geometries, hollow fiber membrane module is more frequently used, because its surface to volume ratio is more than that of other types of membranes [10]. For this purpose, ultra-thin dense palladium deposits on $\alpha - Al_2O_3$ hollow fiber membrane are of more interest, which decrease cost and increase hydrogen permeability [11].

The first model of membrane for gas separation was developed by Waller and Steiner [12]. In 1983, Pan studied a mathematical model for predicting Helium recovery from natural gas by hollow fiber membrane. The effect of permeate-feed flow pattern on module performance was examined [13]. Le et al. developed a mathematical model for gas separation involving 3 or more permeable components. They examined the effects of operating conditions, such as pressure drop across membrane, the stage cut, and flow patterns [14]. The orthogonal collocation method for hydrogen separation from refinery gas was studied by Kaldis et al. [15]. Takaba and Nakao used CFD for hydrogen separation form $H_2$/CO gas mixture by porous ceramic membrane [16]. Chen and Hsu used CFD method to investigate hydrogen separation from nitrogen by 3 different palladium membranes in unsteady state. They analyzed the operating conditions, such as pressure and temperature, by passing time. Also, the optimal pressure exponent of hydrogen diffusion equation in Pd membrane was obtained [17]. Coroneo et al. used CFD modeling of inorganic membranes, such as palladium and ceramic membranes, for hydrogen separation in different configurations and determined the dominant mechanism in the inorganic membrane [18]. Dehkordi et al. considered a mathematical model for gas mixture separation by hollow fiber membrane in non-ideal condition that affected the performance of gas permeator [19]. Wei-Hsin Chen et al. studied the influence of flow pattern and geometry on hydrogen separation from hollow fiber membrane [20].

In this work, the effects of different operation conditions on hydrogen separation by palladium hollow fiber membrane are examined by 3D steady and unsteady modeling. By using computational fluid dynamics, two sets of equations, namely, Navier-Stocks and continuity, are solved.

## 2. Model Development

To predict hydrogen concentration and velocity profile, continuity, Navier-Stokes, and species equations are used, simultaneously. The considered assumptions in the model are as follows (Table 1):

1. Membrane thickness is equal to zero.
2. Nitrogen diffusion is negligible.
3. Module temperature is constant.
4. The concentration profile in tube side is negligible and the pressure (partial pressure of $H_2$) is considered constant, because Nitrogen diffusion through membrane is zero.
5. Fully developed laminar flow is considered.
6. Chemical reaction between hydrogen and Nitrogen does not occur.

**Table 1.** Assumptions of membrane module simulation

| | |
|---|---|
| $H_2$ pressure in tube side | Constant and equal to 1 bar |
| $N_2$ diffusion in membrane | Zero |
| Membrane thickness | Zero |
| Flow regime in shell side | Laminar flow |
| Module temperature | Constant |
| Chemical reaction | Negligible |

Fig. 1 shows the geometry of membrane module. As can be seen, the membrane module is divided into 3 sections: shell, membrane, and tube.

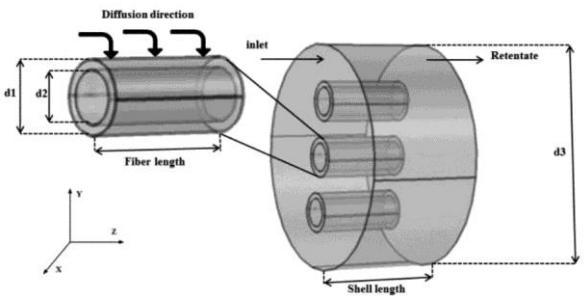


**Figure 1.** Geometry of membrane module

### 2.1. Shell side equations

#### 2.1.1. Partial continuity in shell side

Hydrogen concentration profile is obtained by solving partial continuity. Partial continuity equation in shell side is as follows:

$$\frac{\partial C_i}{\partial t}+\nabla(-D_i\nabla C_i)+u\nabla C_i=0 \quad (1)$$

$$N_i=-D_i\nabla C_i+uC_i \quad (2)$$

where $D_i$, $u$, $C_i$, and $N_i$ denote the diffusion coefficient, bulk velocity, concentration of species I, and diffusion flux, respectively. Boundary conditions for partial continuity equation are as follows:

$$Z=0 \qquad C_i=C_0 \quad (3)$$

$$Z=L \qquad -n.D_i\nabla C_i=0 \quad (4)$$

$$r=\frac{d_1}{2}$$

$$n.N_i=Q_0.\exp(-\frac{E}{RT}).(\mathrm{P}^{\beta}_{H2,shell}-\mathrm{P}^{\beta}_{H2,tube})[21] \quad (5)$$

$$r=\frac{d_3}{2} \qquad -n.N_i=0 \quad (6)$$

In thick palladium membrane, when β is equal to 0.5, surface processes, such as adsorption and dissociation of the hydrogen, are very faster than hydrogen diffusion through the membrane. Hence, mass transfer is controlled by membrane. On the other hand, mass transfer resistance decreases by reducing membrane thickness. Therefore, when the value of β is equal to 1, surface process resistance is more important than membrane resistance. When both of the mechanisms control mass transfer in membrane, $0.5\langle\beta\langle 1$ [5].

The values of $Q_0$ and $E$ in Eq. 5 are equal to $3.12\times10^{-5}\ mol/m^2.pa.s$ and 13900 $mol/J$, which were experimentally obtained by Wang et al. (2006) [21].

#### 2.1.2. Navier-Stokes equations in shell side

Naveir-Stokes equations are used in the model as follows:

$$\rho\frac{\partial u}{\partial t}+\rho(u.\nabla)u=\nabla.\left[-P+\mu\left(\nabla u+(\nabla u)^T\right)\right] \quad (7)$$

$$\rho\nabla.u=S' \quad (8)$$

where $\rho$, $\mu$, and S' denote the density, viscosity of hydrogen, and source term, respectively. Assuredly, the value of S' in the shell side is considered zero. The source term on the right-hand side of Eq. 8 reflects the mass disappearance due to hydrogen transport in the cells adjacent to membrane wall. Assuredly, this source term is zero for the remaining cells in the shell side. The boundary conditions are shown in the following equations for laminar flow as follows:

$$Z=0 \quad u_{0,x}=0 \qquad u_{0,y}=0 \qquad u_{0,z}=2\times u_{ave}\times\left(1-\frac{x^2+y^2}{\left(\frac{d_3}{2}\right)^2}\right) \quad (9)$$

$$Z=L \qquad P=P_0,\left[\mu\left(\nabla u+(\nabla u)^T\right)\right]n=0 \quad (10)$$

### 2.2. Computational approach

Modeling of palladium hollow fiber membrane is performed by solving continuity and Navier-Stokes equations by using computational fluid dynamics method. The simulation has been performed by COMSOL Multiphysics 4.4. For solving equations; *GMRES* solver in steady state and *MUMPS* solver in unsteady state are used. Calculation error is equal to $10^{-4}$ and time step in unsteady state is equal to $10^{-3}$. For calculating two sets of equations, meshing of membrane module is required. For this purpose, the size of grid element near surface membrane is the smallest, since changes of hydrogen concentration and velocity near membrane are high. Triangular mesh element and model geometry are shown in Fig. 2. The mesh consists of 179938 cells.

Due to three-dimensional geometry of module, calculation time increases in comparison with two-dimensional ones. In order to reduce the computational time, the system has been scaled 60000 times along the z-direction and 2000 times along the r-direction. In addition to scale size of module, velocity and diffusion coefficient in shell side should be scaled, which are as follows:

As the cross section of module is circular, the following relation is obtained.

$$scale_x^2 + scale_y^2 = scale_r^2 \quad (11)$$

Also, because the cross section is symmetric, $scale_x$ is equal to $scale_y$; consequently, the following relation is obtained.

$$scale_x = scale_y = \frac{scale_r}{\sqrt{2}} \quad (12)$$

Now, Eq. 14 is achieved by inserting Eq. 12 in the following matrix:

$$D'_{H_2/N_2} = \begin{bmatrix} (\frac{D_{H_2/N_2}}{scale_x^2}) & 0 & 0 \\ 0 & (\frac{D_{H_2/N_2}}{scale_y^2}) & 0 \\ 0 & 0 & (\frac{D_{H_2/N_2}}{scale_z^2}) \end{bmatrix} \quad (13)$$

$$D'_{H_2/N_2} = \begin{bmatrix} (\frac{D_{H_2/N_2}}{scale_r^2})\times 2 & 0 & 0 \\ 0 & (\frac{D_{H_2/N_2}}{scale_r^2})\times 2 & 0 \\ 0 & 0 & (\frac{D_{H_2/N_2}}{scale_z^2}) \end{bmatrix} \quad (14)$$

As the velocity in the module is in the direction of z-axis, the relation of velocity is obtained by the following equation:

$$u_{0,z} = 2\times(\frac{u_{ave}}{scale_z})\times\left(1-\frac{x^2+y^2}{\left(\frac{d_3}{2}\right)^2}\right) \quad (15)$$

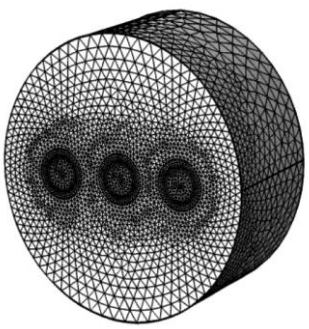

**Figure 2.** Triangular mesh element and model geometry

## 2.3. Model validation

The results are compared with experimental data, which were reported by Wang et al. (2006). The effective area and length of each membrane are equal to 1.5cm$^2$ and 4.5cm, respectively. As mentioned in the report by Wang et al., 3 membranes in the module are considered. The thermocouple is used to control temperature and heat of tubular furnace. By using permeation data of pure gas in membrane, the constants required in modeling, such as activation energy, pre-exponential factor, and pressure exponent $(\beta)$, are obtained from the mentioned article. The $H_2/N_2$ ratio is set to 1:1 in gas mixture. Also, the thickness of Pd layer is equal to 2-3 $\mu m$ that is coated on $\alpha/Al_2O_3$ hollow fiber membrane. Since the thickness of palladium membrane is low, the surface process mechanism controls mass transfer in Pd membrane and the value of $\beta$ in Eq. 5 is equal to 1.

The specifications of module membrane include inner and outer diameters of membrane and diameter of shell, which are equal to 500, 700, 4000 μm, respectively; also, the lengths of shell and membrane are equal to 6 and 4.5 cm, respectively (Table 2).

**Table 2.** Specifications of membrane module

| | |
|---|---|
| Shell diameter (μm) | 4000 |
| Outer membrane diameter (μm) | 700 |
| Inner membrane diameter (μm) | 500 |
| Module length (cm) | 6 |
| Membrane length (cm) | 4.5 |
| Number of membranes | 3 |
| Scale factor of length | 60000 |
| Scale factor of radius | 2000 |
| Dimensions of module | 3 |

In Fig. 3, the effect of temperature on the removal of hydrogen in different feed flow rates and in steady state is examined. According to Eq. 5, increasing the temperature results in enhancing hydrogen separation. This fact is only seen in the flow rate of 200 ml/min. It could be related to the fact that at lower flow rates (below 200 ml/min), the difference between the permeate and the shell side is not large enough to quickly reach the equilibrium state and the effect of temperature on hydrogen separation is not considerable. By increasing the feed flow rate, driving force increases and, then, equilibrium state occurs; therefore,

the effect of temperature is significant in the flow rate equal to 200 ml/min. The results show good agreement with experimental data.

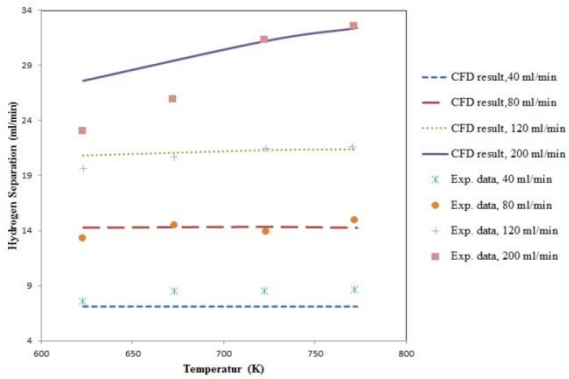


**Figure 3**. Effect of temperature on hydrogen removal in different feed flow rates ($\Delta p = 1.6\ bar$)

## 3. Results and Discussion

In this section, the transient hydrogen flux across a Pd membrane at various pressures and temperatures is studied.

Fig. 4 shows profile of velocity in shell side and steady state. As it can be seen, velocity between fibers is the lowest, because of less space for passing of gas mixture.

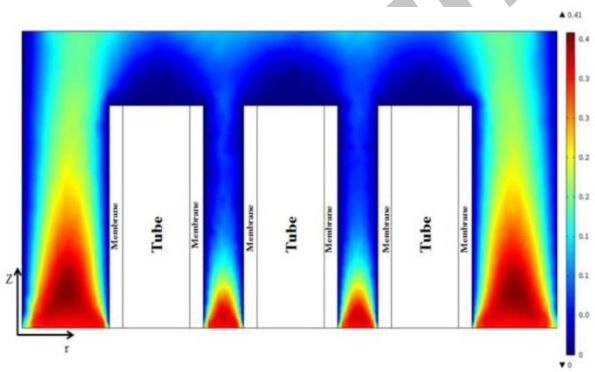


**Figure 4.** Distribution of bulk velocity in the shell side

Fig. 5 shows direction of hydrogen flux in the cut plane of shell in steady-state condition. According to this figure, direction of hydrogen flux is toward membrane due to hydrogen concentration difference between shell and tube side.

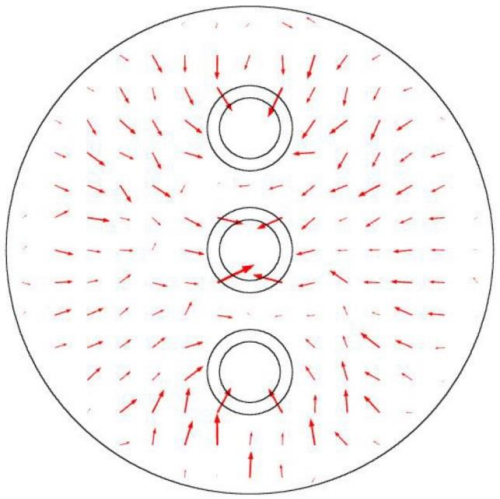

**Figure 5.** Direction of hydrogen flux in the cut plane of shell

The steady-state hydrogen concentration profile in the shell is shown in Fig. 6. Variation of hydrogen concentration between fibers is the most due to the fact that the velocity between fibers decreases and, consequently, residence time and hydrogen separation increase. Moreover, due to the high permeability of hydrogen in palladium membrane, hydrogen separation mostly occurs at the begging of shell side.

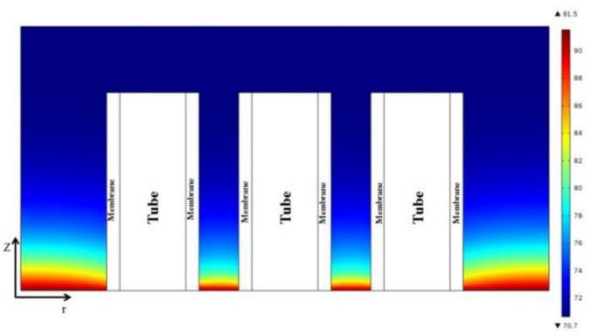


**Figure 6.** Distribution of Hydrogen concentration in the shell side

In Fig. 7, the comparison between straight line and triangular configuration in various pressures is shown. According to this figure, by increasing the pressure, $H_2$ separation in triangular configuration is more than that in straight line, because the concentration polarization effect in straight line configuration is more than that in triangular configuration.

Profiles of hydrogen concentration are shown at different times in Fig. 8. As can be seen, by passing time, amount of hydrogen decreases in the shell side, because hydrogen penetrates through the membrane.

Trends of hydrogen flux versus time at various temperatures are shown in Fig. 9 at two feed flow rates of 40 and 200 ml/min. As can be seen in this figure, the profile has two distinct stages in each temperature. In the first stage, the trend has a sharp and negative slope, in which hydrogen penetrates through the membrane in unsteady condition and the amount of hydrogen decreases in the shell side. In the second stage, the slope is near zero and it corresponds to the steady condition. According to this figure, by increasing the temperature, the slope of the first section becomes sharper and steady condition occurs sooner. The results can be related to the fact that higher temperature results in more hydrogen permeation across the membrane based on Eq. 5. By comparing Figs. 9(a) and 9(b), it can be concluded that changing temperature at higher feed flow rates is more important than in lower feed flow rates. Since time resident decreases by increasing feed flow rate, equilibrium state happens later. As a result, the hydrogen permeation across the membrane is more sensitive to temperature at higher feed flow rates.

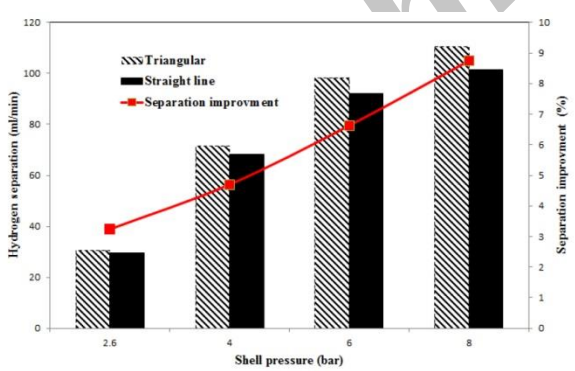


**Figure 7.** The effect of triangular and straight line configurations on hydrogen separation ($T = 773\ K \& F = 200\ ml/\text{min}$)

Fig. 10 shows hydrogen partial pressure difference between shell and tube side versus time at constant total pressure, which is equal to 2.6 bar. As can be seen in this figure, the changes of pressure difference versus time are opposite to the hydrogen flux changes in Fig. 9. As mentioned, the hydrogen flux is lower at low temperatures; therefore, partial pressure of hydrogen is increased in the shell side. As a result, pressure difference between shell and tube side increases at lower temperatures.

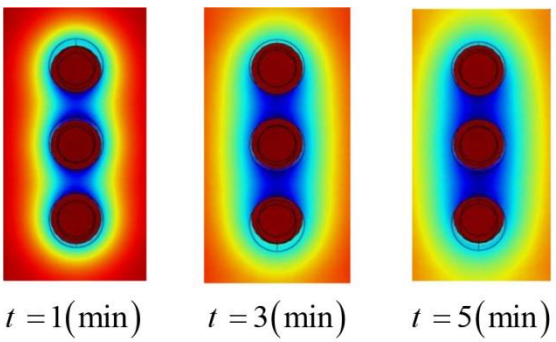


**Figure 8.** Distribution of transient hydrogen concentration in the shell side

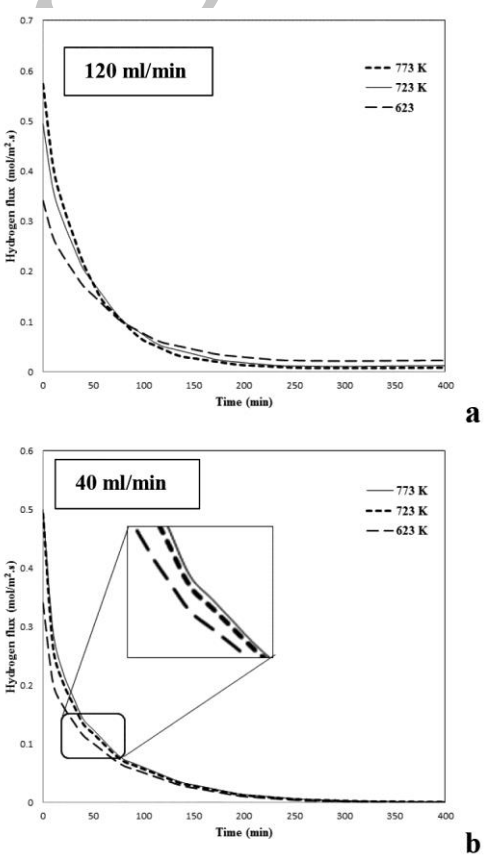


**Figure 9.** Hydrogen flux through membrane at different temperatures

The time required to reach 1% of the initial flux through membrane is called quasi-steady time $(t_{99})$. Using quasi-steady time, the influences of

various operation conditions on hydrogen separation can be compared with each other. In Fig. 11, the effect of temperature on quasi-steady time $(t_{99})$ is examined at constant feed flow rate and pressure. As can be seen, the value of $t_{99}$ is between 251 and 253 at three different temperatures. By increasing temperature, the quasi-steady time is shorter due to the fact that hydrogen flux through membrane increases. This could be another reason for sudden flux drop at higher temperatures.

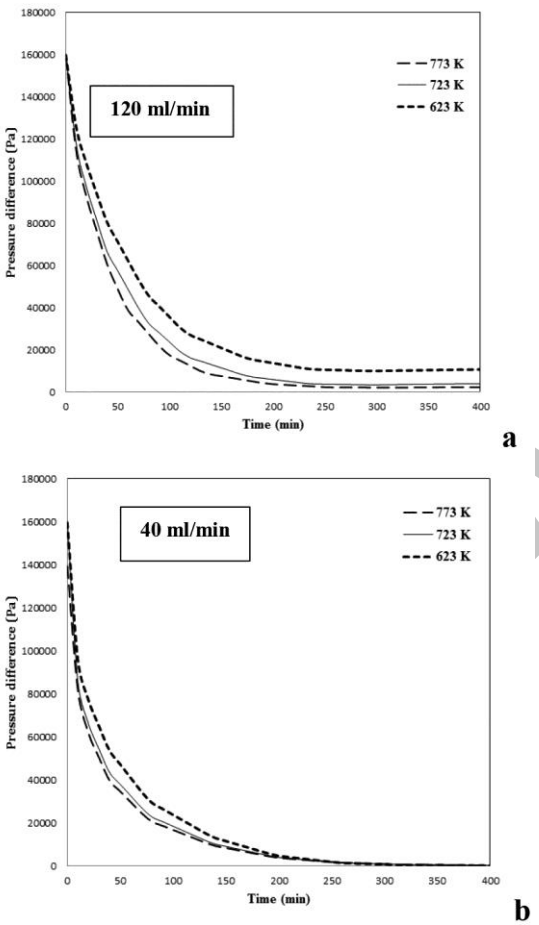


**Figure 10.** Pressure difference between shell and tube side versus time

The time required to reach 50% of initial flux through membrane is called half-steady time $(t_{50})$. Useful information (fraction of the time required to reach 50% separation) on the ratio of $t_{99}$ to $t_{50}$ can be obtained. Fig. 12 shows half-steady time versus temperature at various feed flow rates. As shown, by increasing temperature, half-steady time decreases due to the fact that permeability of hydrogen across the membrane increases. When feed flow rate increases, half-steady time increases, because the residence time decreases.

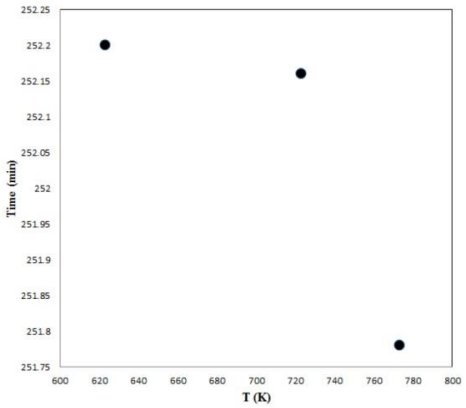


**Figure 11.** The effect of temperature on quasi-steady time at constant pressure and feed flow rate ($p = 2.6\ bar$, $F = 40\ ml/min$)

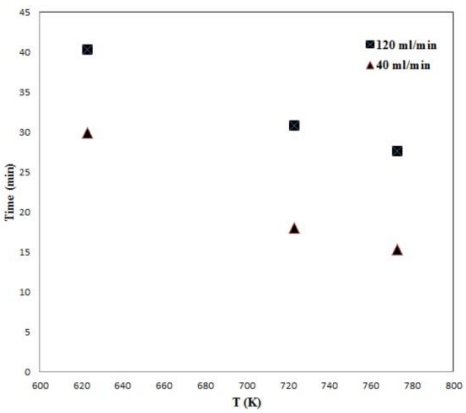


**Figure 12.** Half- steady time versus temperature at constant pressure ($p = 2.6\ bar$)

In Fig. 13, the effect of temperature on the ratio of half-steady time to quasi-steady time is studied at constant feed flow rate and pressure. At all investigated temperatures in this paper, ratio of half-steady time to quasi-steady time is lower than 8%. This means that about 50% of hydrogen mass separation is obtained in the initial 8% period of permeation time. In addition, by increasing the temperature, $\frac{t_{50}}{t_{99}}$ decreases.

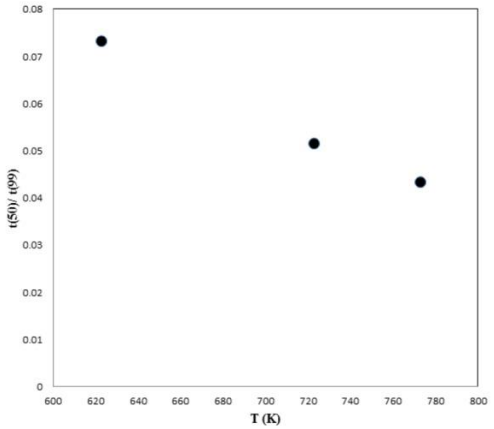


**Figure 13.** The effect of temperature on ratio of half-steady time and quasi-steady time at feed flow rate of 40 $ml/min$

### 3.1. Characteristic time

The contribution of mass resistance between membrane and gas phase can be analyzed by considering characteristic time parameter. Also, characteristic times can help to design and calculate the ratio of surface to volume and thickness of membrane and adjust the feed conditions. In this section, all calculations are based on experimental data, which were obtained by Wang et al. (2006). Characteristic times based on various competing transport processes can be classified in 4 categories, which are defined as follows [22]:

1- Radial diffusion in gas phase

$$\tau_d = \frac{\left(R_2 - R_1\right)^2}{D_{H_2/N_2}} \tag{16}$$

where $R_2$, $R_1$, and $D_{H_2/N_2}$ denote the inner radius of shell, the outer radius of fiber, and diffusion coefficient in gas mixture, respectively.

2- Hydrogen diffusion in metallic bulk of membrane

$$\tau_{pd} = \frac{\delta^2}{D_H(T)} \tag{17}$$

$$D_H = D_H^0 \exp\left(-\frac{E}{\Re T}\right) \tag{18}$$

where $\delta$ represents the thickness of membrane and $D_H$ represents the diffusion of hydrogen atoms in metallic bulk of membrane. The amounts of $E$ and $D_H^0$ are equal to $14175\left(\frac{J}{mol}\right)$ and $9.45\times10^{-8}\left(\frac{m^2}{s}\right)$, respectively [23].

3- Permeation of hydrogen from shell to tube side

$$\tau_p = \frac{C_{H_2}^0}{(S/V)J} = \frac{C_{H_2}^0}{(S/V)(Q/\delta)\Delta P_{H_2}} \tag{19}$$

where $C_{H_2}^0$, $J$, and $Q/\delta$ represent the initial hydrogen concentration in feed side, the hydrogen flux through the palladium membrane, and the permeability, respectively. Also, $S/V$ is equal to $\frac{2R_1}{R_2^2}$.

4- Feed flow rate in the shell side (axial diffusion time)

$$\tau_f = \frac{\pi\left(R_2^2 - R_1^2\right)L_m}{V_0} \tag{20}$$

where $V_0$ denotes the amount of feed flow rate and $L_m$ denotes thickness of support membrane.

As can be seen in the above equations, characteristic times change with temperature, pressure, material, and thickness of membrane. $\tau_p$ and $\tau_d$ are dependent on ratio of surface to volume of module and $\tau_{pd}$ is dependent on membrane thickness. By comparing characteristic times with each other, the dominating resistance can be determined.

Fig. 14 shows $\tau_p$ and $\tau_{pd}$ versus ratio of surface to volume at several palladium membrane thicknesses. By increasing $S/V$, both characteristic times decrease. As can be seen, permeation time increases when membrane thickness increases. This means that diffusion of hydrogen from gas phase to tube side is slower than the radial diffusion in the gas phase. As a result, the permeation in the membrane controls the mass transfer.

In Fig. 15, permeation time $\left(\tau_p\right)$ is compared with feed time $\left(\tau_f\right)$ at different ratios of $S/\mathrm{V}$. By enhancing the surface to volume ratio, $\tau_p$ and $\tau_f$ are reduced. As can be observed in Fig. 15, the values of $\tau_p$ and $\tau_f$ are very different; thus, it can be concluded that the value of $\tau_p$ is more than $\tau_f$ at different thicknesses and flow rates. For this reason, permeation of hydrogen from feed to permeate side controls mass transfer in comparison with axial hydrogen permeation. By decreasing feed flow rate and membrane thickness, the difference between $\tau_p$ and $\tau_f$ decreases. Therefore, the more the flow rate, the less the convection resistance.

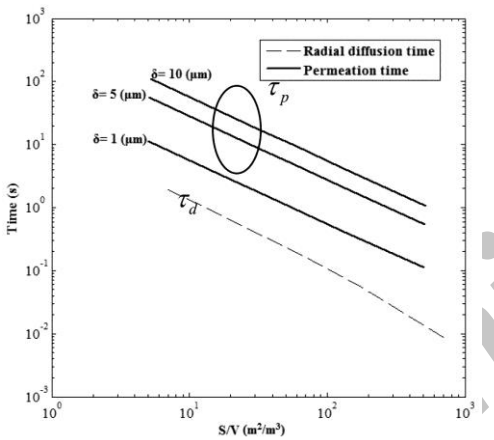


**Figure 14.** $\tau_p$ and $\tau_d$ versus membrane surface to volume ratio

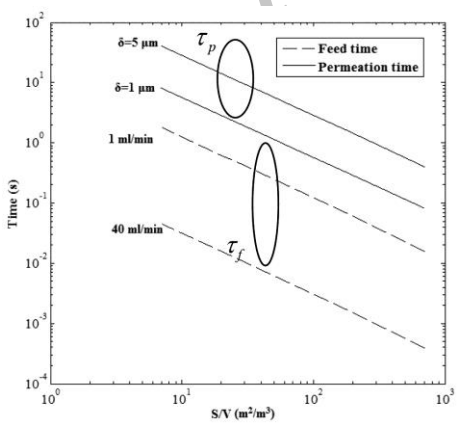


**Figure 15.** Permeation time and feed time versus ratio of surface to volume

In Fig. 16, the characteristic time for metallic bulk of the membrane $\left(\tau_{pd}\right)$ is investigated at different membrane thicknesses. By increasing membrane thickness, characteristic time for metallic bulk of membrane increases, because membrane resistance and pass time increase.

In Fig. 17, the times of membrane diffusion and radial diffusion (radial diffusion in shell side) versus surface to volume ratio are shown. It should be noted that in the design of membrane module, radial diffusion time $\left(\tau_d\right)$ is more than diffusion time in metallic bulk of membrane $\left(\tau_{pd}\right)$; otherwise, the membrane diffusion will control mas transfer. Therefore, the decrease in hydrogen separation is higher than when radial diffusion controls mass transfer. When radial diffusion controls mass transfer, concentration polarization is more important, because concentration gradient occurs in the shell side. If the membrane diffusion time is more than radial diffusion time, the membrane thickness is called critical thickness. Considering these figures, by using the coordinate collision, critical thickness of membrane can be obtained at constant pressure (2.6 bar) and temperature (773 K). It should be noted that computational fluid dynamics for calculating $\tau_{pd}$ and $\tau_d$ are not required. The critical thickness of membrane is equal to 12 $\mu m$, which is in good agreement with the value given by Gielens et al. [24].

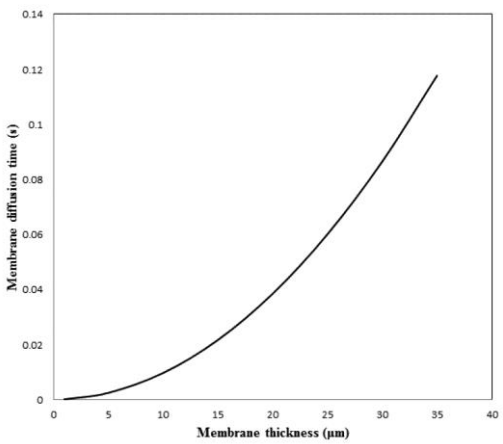


**Figure 16.** Membrane diffusion time versus thickness of membrane

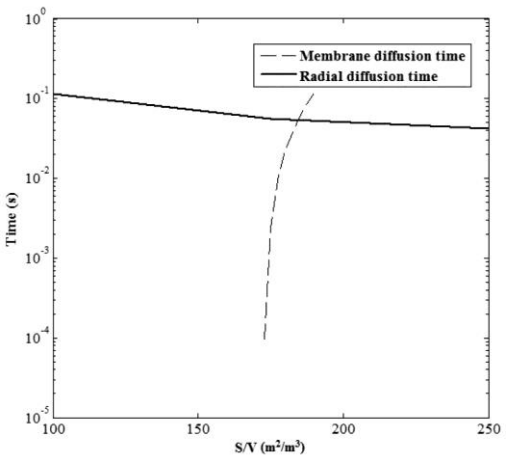


**Figure 17.** Membrane diffusion time and radial diffusion time versus surface to volume ratio

## 4. Conclusion

In this paper, the influence of operating conditions on hydrogen flux through the membrane was investigated by passing time. The membrane module included 3 hollow fiber membranes through which feed stream entered shell side. The velocity between fibers was the lowest. In the other words, residence time for hydrogen separation between fibers was more. By increasing the temperature, hydrogen permeability of membrane increased so that flux drop of hydrogen increased by passing time. According to the results, about 50% hydrogen mass separation was obtained in the initial 8% period of permeation time. The contribution of resistance between the membrane and the gas phase could be analyzed by considering characteristic times. When the thickness of palladium membrane was more than 1μm, the permeation time was more than radial and feed time. Thus, the hydrogen permeation from shell to tube side controlled mass transfer in comparison with radial and feed permeation. As mentioned, when thickness of membrane was overcritical, bulk metal of membrane controlled mass transfer, which was calculated equal to 12μm. As a result, when thickness of membrane was less than critical thickness, the surface process resistance was important.

## Nomenclature

| | |
|---|---|
| $C_i$ | Concentration of species i, mol m$^{-3}$ |
| $C^0_{H_2}$ | Initial concentration of hydrogen, mol m$^{-3}$ |
| $D_i$ | Diffusivity, m$^2$ s$^{-1}$ |
| $D_H$ | Hydrogen diffusion in palladium membrane, m$^2$ s$^{-1}$ |
| $D^0_H$ | Hydrogen diffusion constant in palladium membrane, m$^2$ s$^{-1}$ |
| $D_{H_2/N_2}$ | Hydrogen diffusion in $H_2$ and $N_2$ mixture, m$^2$ s$^{-1}$ |
| E | Activation energy of atomic hydrogen diffusion coefficient, J mol$^{-1}$ |
| $E_A$ | Apparent activation energy, J mol$^{-1}$ |
| $F_{H_2}$ | Flux of hydrogen through membrane, mol m$^{-2}$ s$^{-1}$ |
| K | Hydrogen permeation in palladium membrane, mol m$^2$ s$^{-1}$ Pa$^{-\beta}$ |
| L | Module length, m |
| $L_m$ | Thickness of support membrane, m |
| N | Normal vector, dimensionless |
| $N_i$ | Diffusion flux, mol m$^{-2}$ s$^{-1}$ |
| P | Pressure, Pa |
| $P_0$ | Initial pressure, Pa |
| $P_{r,H_2}$ | Partial pressure of hydrogen in retentate side, Pa |
| $P_{p,H_2}$ | Partial pressure of hydrogen in permeate side, Pa |
| $P_{H_2,shell}$ | Partial pressure of hydrogen in shell side, Pa |
| $P_{H_2,tube}$ | Partial pressure of hydrogen in tube side, Pa |
| $Q_0$ | Pre-exponential factor, mol m$^{-2}$ s$^{-1}$ Pa$^{-\beta}$ |
| $\Re$ | Ideal gas constant, J mol$^{-1}$ K$^{-1}$ |
| $R_1$ | Membrane's outer radius, m |
| $R_2$ | Membrane's inner radius, m |
| $R_3$ | Shell radius, m |
| T | Temperature, K |
| T | Time, s |
| U | Bulk velocity, m s$^{-1}$ |
| $u_{ave}$ | Average velocity of bulk, m s$^{-1}$ |
| S' | Source term in Navier-Stokes equations |
| $Scale_x$ | Scale factor (x-axis), dimensionless |
| $Scale_y$ | Scale factor (y-axis), dimensionless |
| $Scale_z$ | Scale factor (z-axis), dimensionless |
| $Scale_r$ | Scale factor (r-axis), dimensionless |
| $V_0$ | Feed flow rate, m$^3$ s$^{-1}$ |
| S/V | Ratio of surface to volume, m$^{-1}$ |
| $\Delta p_{H_2}$ | Hydrogen pressure difference between feed and permeate side, Pa |

## Greek symbols

| | |
|---|---|
| $\tau_d$ | **Radial diffusion time, s** |
| $\tau_p$ | Permeation diffusion time, s |
| $\tau_{pd}$ | Membrane diffusion time, s |
| $\tau_f$ | Feed diffusion time, s |
| β | Exponent of pressure, dimensionless |
| $\delta$ | Thickness of membrane, m |
| $\rho$ | Density, Kg m$^{-3}$ |

## References

[1] Baker, R.W. (2002). "Future directions of membrane gas separation technology." *Industrial & Engineering Chemistry Research*, Vol. 41 (6), pp. 1393-1411.

[2] Phair, J.W. and Badwal, S.P.S. (2006). "Materials for separation membranes in hydrogen and oxygen production and future power generation." *Science and Technology of Advanced Materials*, Vol. 7 (8), pp. 792-805.

[3] Basile, A. (2008). "Hydrogen production using Pd-based membrane reactors for fuel cells." *Topics in Catalysis*, Vol. 51 (1-4), p. 107.

[4] Chen, W.H. and Hsu, P.C. (2011). "Hydrogen permeation measurements of Pd and Pd–Cu membranes using dynamic pressure difference method." *International Journal of Hydrogen Energy*, Vol. 36 (15), pp. 9355-9366.

[5] Gallucci, F., Chiaravalloti, F., Tosti, S., Drioli, E. and Basile, A. (2007). "The effect of mixture gas on hydrogen permeation through a palladium membrane: experimental study and theoretical approach." *International Journal of Hydrogen Energy*, Vol. 32 (12), pp. 1837-1845.

[6] Gao, H., Lin, Y.S., Li, Y. and Zhang, B. (2004). "Chemical stability and its improvement of palladium-based metallic membranes." *Industrial & Engineering Chemistry Research*, Vol. 43 (22), pp. 6920-6930.

[7] Chen, C. H. and Ma, Y.H. (2010). "The effect of H2S on the performance of Pd and Pd/Au composite membrane." *Journal of Membrane Science*, Vol. 362 (1), pp. 535-544.

[8] Tosti, S., Basile, A., Borelli, R., Borgognoni, F., Castelli, S., Fabbricino, M., Gallucci, F. and Licusati, C. (2009). "Ethanol steam reforming kinetics of a Pd–Ag membrane reactor." *International Journal of Hydrogen Energy*, Vol. 34, No. 11, pp. 4747-4754.

[9] Yang, J.Y., Komaki, M. and Nishimura, C. (2007). "Effect of overlayer thickness on hydrogen permeation of Pd60Cu40/V–15Ni composite membranes." *International Journal of Hydrogen Energy*, Vol. 32 (12), pp. 1820-1824.

[10] Chen, W.H., Hsia, M.H., Lin, Y. L., Chi, Y.H. and Yang, C.C. (2013). "Hydrogen permeation and recovery from H2–N2 gas mixtures by Pd membranes with high permeance." *International Journal of Hydrogen Energy*, Vol. 38 (34), pp. 14730-14742.

[11] Pan, X.L., Xiong, G.X., Sheng, S.S., Stroh, N. and Brunner, H. (2001). "Thin dense Pd membranes supported on α-Al2O3 hollow fibers." *Chemical Communications*, No. 24, pp. 2536-2537.

[12] Weller, S. and Steiner, W.A. (1950). "Separation of gases by fractional permeation through membranes." *Journal of Applied Physics*, Vol. 21 (4), pp. 279-283.

[13] Pan, C.Y. (1983). "Gas separation by permeators with high-flux asymmetric membranes." *AIChE Journal*, Vol. 29 (4), pp. 545-552.

[14] Li, K., Acharya, D.R. and Hughes, R. (1990). "Mathematical modelling of multicomponent membrane permeators." *Journal of Membrane Science*, Vol. 52 (2), pp. 205-219.

[15] Kaldis, S.P., Kapantaidakis, G.C. and Sakellaropoulos, G.P. (2000). "Simulation of multicomponent gas separation in a hollow fiber membrane by orthogonal collocation—hydrogen recovery from refinery gases." *Journal of Membrane Science*, Vol. 173 (1), pp. 61-71.

[16] Takaba, H. and Nakao, S.I. (2005). "Computational fluid dynamics study on concentration polarization in H 2/CO separation membranes." *Journal of Membrane Science*, Vol. 249 (1), pp. 83-88.

[17] Chen, W.H. and Hsu, P.C. (2011). "Hydrogen permeation measurements of Pd and Pd–Cu membranes using dynamic pressure difference method." *International Journal of Hydrogen Energy*, Vol. 36 (15), pp. 9355-9366.

[18] Coroneo, M., Montante, G., Baschetti, M. G. and Paglianti, A. (2009). "CFD modelling of inorganic membrane modules for gas mixture separation." *Chemical Engineering Science*, Vol. 64 (5), pp. 1085-1094.

[19] Dehkordi, J.A., Hosseini, S.S., Kundu, P. K. and Tan, N.R. (2016). "Mathematical Modeling of Natural Gas Separation Using Hollow Fiber Membrane Modules by Application of Finite Element Method through Statistical Analysis." *Chemical Product and Process Modeling*, Vol. 11, (1), pp. 11-15.

[20] Chen, W.H., Syu, W.Z., Hung, C. I., Lin, Y.L. and Yang, C.C. (2013). "Influences of geometry and flow pattern on hydrogen separation in a Pd-

based membrane tube." *International Journal of Hydrogen Energy*, Vol. 38 (2), pp. 1145-1156.

[21] Wang, W.P., Thomas, S., Zhang, X.L., Pan, X.L., Yang, W.S. and Xiong, G.X. (2006). "H2/N2 gaseous mixture separation in dense Pd/α-Al2O3 hollow fiber membranes: experimental and simulation studies." *Separation and purification technology*, Vol. 52 (1), pp. 177-185.

[22] Nair, B.K.R. and Harold, M.P. (2008). "Experiments and modeling of transport in composite Pd and Pd/Ag coated alumina hollow fibers." *Journal of Membrane Science*, Vol. 311 (1), pp. 53-67.

[23] Caravella, A., Scura, F., Barbieri, G. and Drioli, E. (2010). "Inhibition by CO and polarization in Pd-based membranes: a novel permeation reduction coefficient." *The Journal of Physical Chemistry B*, Vol. 114, (38), pp. 12264-12276.

[24] Gielens, F.C., Knibbeler, R.J.J., Duysinx, P.F.J., Tong, H.D., Vorstman, M. A.G. and Keurentjes, J. T. F. (2006). "Influence of steam and carbon dioxide on the hydrogen flux through thin Pd/Ag and Pd membranes." *Journal of Membrane Science*, Vol. 279 (1), pp. 176-185.